


# A dual quantum image feature extraction method: PSQIFE

Jie Su<sup>1</sup>  | Shuhan Lu<sup>2</sup> | Lin Li<sup>1</sup><sup>1</sup>College of Information and Electrical Engineering, China Agricultural University, Beijing, China<sup>2</sup>Master of Health Informatics, School of Information, University of Michigan, Ann Arbor, Michigan, USA**Correspondence**Jie Su and Lin Li, College of Information and Electrical Engineering, China Agricultural University, Beijing 100083, China.  
Email: sujiework@cau.edu.cn; lilinli@cau.edu.cn**Funding information**

National Key Research and Development Project of China, Grant/Award Number: 2016YFD0300710

**Abstract**

In digital image processing, feature extraction occupies a very important position, which is related to the effect of image classification or recognition. At present, effective quantum feature extraction methods are relatively lacking. And the current feature extraction methods are mainly devoted to the extraction of basic features of images, failing to consider the global features of classical images and the global features of quantum images comprehensively. In this paper, we propose a dual quantum image feature extraction method named PSQIFE, which focuses on the global energy representation of images by constructing dual quantum image global features. The representation of the global features of the dual quantum image is obtained by quantum superposition of two parts of quantum state features. In this paper, quantum image reconstruction and quantum image fidelity tests are performed on the extracted global features by 9 classes of classical images, and the overall fidelity is above 95%. In addition, the effectiveness of PSQIFE dual quantum image feature extraction method is verified by comparing the image classification test with convolutional feature extraction method on Mnist dataset. The method has some reference significance for the research of quantum image feature extraction and classification.

## 1 | INTRODUCTION

In the era of big data, the generation of image data is exponentially exploding, and it is a very important issue to organize and manage these large-scale data effectively and to explore the potential value of these big data for image-related applications [1–4], such as classification and labelling of images [5, 6]. Features have a very important position in image classification, which is related to the efficiency of image classification, and likewise, the research of quantum image feature extraction methods is also very critical.

Image features contain two major categories, the first one is the basic features consisting of shape, colour and texture, and the second one is the semantic features such as scene and behaviour. In practical problem processing, image feature extraction can improve the efficiency of image processing by invariant features of images. The common classical image feature extraction methods mainly focus on the extraction of local or global features of images, and the related methods include colour feature extraction methods, texture feature extraction methods, shape feature extraction methods and spatial rela-

tionship feature extraction methods and other artificial feature extraction methods. The representative artificial feature extraction methods are Local Binary Patterns (LBP), Scale-Invariant Feature Transform (SIFT) and Histogram of Oriented Gradient (HOG). In addition, automatic feature extraction includes linear and non-linear feature transformations, supervised and unsupervised feature transformations, such as Principal Component Analysis (PCA), Canonical Correlation Analysis (CCA), manifold learning, kernel methods, and deep learning methods etc. Among them, Support Vector Machines (SVM) in kernel methods, Convolutional Neural Networks (CNN), Recurrent Neural Network (RNN) and Transformer in deep learning have strong feature learning capability [7–12]. Since these classical image feature extraction methods cannot be directly used in the field of quantum image processing, it is necessary to study quantum image feature extraction methods.

In the face of this problem, the following scholars have conducted related researches in quantum feature extraction methods. Yu et al. proposed a sparse feature extraction method based on quantum evolutionary algorithm to achieve the extraction of internal features of signals [13]. Wang proposed a

quantum algorithm for image edge information detection, which can be implemented on quantum computers of different architectures [14]. In order to improve the quality of image edge feature extraction, Tian et al. adopted quantum kernel clustering algorithm and tested the extraction of image edge features through simulation experiments with clear feature contours and good coherence [15]. Zhang superimposed feature points with equal weights for NEQR quantum images and used quantum counting to obtain the number of feature points in the quantum superposition state [16]. Cao combines Fisher classifier with SVM and proposes IBQPSO algorithm, which can realize global search and feature extraction [17]. Li proposes a new QNN algorithm that greatly reduces the learning speed and conducts fingerprint recognition research based on this method [18]. Zhang proposed a collaborative neural network based on quantum evolutionary planning, which can perform feature extraction to accomplish multi-category recognition [19]. Wu experimentally derived the effectiveness of M-FastICA method for face recognition [20]. Zhou et al. achieved pattern feature extraction with the help of quantum parallelism property and quantum Fourier transform, which has exponential acceleration compared with traditional methods [21]. In addition, some scholars are currently working on the automatic extraction of features through quantum convolutional neural networks, which mainly implement the relevant functions of classical convolutional neural networks through quantum circuits and train the networks by updating the parameters of quantum gates in quantum circuits through classical optimization algorithms, so as to achieve efficient extraction and learning of image features [22–25]. The feature extraction methods in these studies are mainly devoted to the extraction of the basic features of images, and fail to consider the global features of classical images and the global features of quantum images comprehensively; in addition, the fidelity of quantum images after the extraction of quantum image features has not been studied and analyzed. Therefore, it is necessary to explore the extraction methods of global features of dual-modal quantum images based on classical images and quantum images for image classification needs.

A comprehensive analysis shows that the main problems are as follows: (1) Classical image feature extraction algorithms cannot be directly applied to quantum image processing and need to be modified by quantum algorithms; (2) the feature extraction methods in the current study fail to consider the global features of classical images and quantum images; (3) there are limitations for quantum images with different quantum encodings and cannot be directly applied to INCQI quantum images for image classification tasks; (4) the fidelity of quantum images after quantum image feature extraction is not considered.

To address the above problems, this paper proposes to construct a dual-quantum image feature extraction method PSQIFE, which fully considers the global features of classical image features and INCQI quantum images with better fidelity and can improve the quantum image classification effect. The method mainly analyzes the statistical-based feature extraction methods in classical images, selects the classical

PCA coefficients as the quantum feature encoding of images, and combines the high-order tensor SVD-Schmidt decomposition technique in quantum many-body problems to construct a dual quantum image feature extraction method PSQIFE, which speeds up the unitary matrix in quantum image feature extraction processing speed. The PSQIFE method is proved to be effective for the global feature representation of quantum images and the processing efficiency is greatly improved by experiments.

The rest of this paper is organized as follows. Section 2 describes the related work. Section 3 describes the PSQIFE quantum image extraction algorithm. Section 4 shows the experiments. Section 5 shows the conclusion.

## 2 | RELATED WORKS

### 2.1 | PCA and quantum feature coding

A part of the quantum image features in this paper is derived from the quantum state encoding of the classical image features obtained after the PCA transformation of the classical image. PCA was proposed in 1901, and it is able to perform the analysis of multivariate statistical distributions. In the field of pattern recognition, this method has been widely used with remarkable recognition results. Improvements based on PCA have emerged such as ICA, KPCA, 2DPCA algorithms etc. They mainly use statistical information of images, and these improvements have improved the recognition effect to some extent, but at the same time increased the computational complexity and space complexity [26–28]. In addition, PCA combined with HMM or ANN, which are methods of pattern recognition, can be used for classification and recognition. These classical methods have a large spatial spend in performing feature space calculations and can be used for quantum image feature extraction operations by quantum improvement. This section focuses on the encoding of quantum features by PCA coefficients.

In classical image processing, the process of feature extraction by PCA and used for image classification mainly consists of two stages: training and classification. Usually the same class of images often has similar features, which can be expressed by PCA. The general steps of PCA operation are shown below.

For the training phase, suppose there are  $K$  grayscale images of size  $M \times N$  in the training set, and each image matrix is rearranged into a column vector, then the whole training set will constitute a matrix  $X$  with  $M \times N$  rows and  $K$  columns. The PCA training phase is shown as Table 1.

After obtaining the feature space, these feature spaces constitute a library of pattern features that can be used for similarity matching in subsequent classification recognition. The steps of the classification and identification stage are shown below (see Table 2).

The  $i$ th feature of the  $j$ th image target in the classical PCA algorithm can be written as  $u_i^T d_j$ . Then the  $i$ th feature of all image targets in the whole database is  $\mu_i^T (d_1, d_2, \dots, d_K)$ , that is,  $\mu_i^T A$ . Where  $u_i^T d_j$  satisfies  $-\sqrt{\lambda_i} \leq u_i^T d_j \leq \sqrt{\lambda_i}$ .

**TABLE 1** The process of PCA

Input: The training set  $X = (x_1, x_2, \dots, x_K)$ .  
 Output: The feature space  $W$

- Step 1: Calculate the mean value by  $\phi = \frac{1}{K} \sum_{i=1}^K x_i$ .  
 Step 2: Calculate the difference from the mean value by  $d_i = x_i - \phi$ .  
 Step 3: Construct the covariance matrix, and get  
 $C = \frac{1}{K} \sum_{i=1}^K d_i d_i^T = \frac{1}{K} A A^T$ , where  $A = (d_1, d_2, \dots, d_K)$ .  
 Step 4: Calculate the eigenvalues and eigenvectors of matrix  $C$ , and select the  $p$  largest eigenvalues by  $\psi = \frac{\sum_{i=1}^p \lambda_i}{\sum_{i=1}^K \lambda_i} \geq \alpha$ , where  $\psi$  is called the contribution rate and  $\alpha$  is generally taken as 99%.  
 Step 5: Get the eigenvectors of  $A A^T$  and the corresponding eigenspaces by  $\mu_i = \frac{1}{\sqrt{\lambda_i}} A v_i$  and  $W = (\mu_0, \mu_1, \dots, \mu_{p-1})$ .

**TABLE 2** The process of classification

Input: the test image  $\Gamma$ , The feature space  $W$ .  
 Output: the class of  $\Gamma$ .

- Step 1: Find the projection features of the mean difference of the test image  $\Gamma$  in the feature space by  $\Omega = W^T (\Gamma - \phi)$ .  
 Step 2: Use Euclidean distance to determine the similarity between the features of the test image and the features  $\Omega_j$  in the pattern feature library by  $\sigma = \|\Omega - \Omega_j\|$ . Comparing  $\sigma$  with the threshold  $\varepsilon$ , the class of the test image  $\Gamma$  can be determined.

Therefore, the  $i$ th feature of the target of the  $j$ th image can be defined as follows:

$$\cos(\theta_i^j) = \frac{\mu_i^T d_j}{\sqrt{\lambda_i}}, \quad \theta_i^j \in [0, \pi] \quad (1)$$

Then all the features of the target of the  $j$ th image can be written in the following form:

$$\left( \cos(\theta_0^j), \cos(\theta_1^j), \dots, \cos(\theta_{p-1}^j) \right) \quad (2)$$

In this way, the similarity determination condition of two image targets can be defined as follows:

$$\left| \cos(\theta_i^j) - \cos(\theta_i^{j'}) \right| < \varepsilon \quad (3)$$

In Equation (3),  $\varepsilon \in (0, 0.5)$ ,  $i = 0, 1, \dots, p - 1$ .

Since the feature values are filtered in descending order from largest to smallest, and the feature values in the new feature  $\cos(\theta_i^j) = \frac{\mu_i^T d_j}{\sqrt{\lambda_i}}$  are divided as the denominator, the important features in the front are “diluted” while the features in the back are enhanced by dividing them by a smaller feature value, so the definition of the new feature can be corrected by dividing it by

the largest feature value uniformly as follows:

$$\cos(\theta_i^j) = \frac{\mu_i^T d_j}{\sqrt{\lambda_0}}, \quad \theta_i^j \in [0, \pi] \quad (4)$$

$$\left| \cos(\theta_i^j) - \cos(\theta_i^{j'}) \right| = \left| \frac{\mu_i^T d_j}{\sqrt{\lambda_0}} - \frac{\mu_i^T d_{j'}}{\sqrt{\lambda_0}} \right| < \varepsilon \quad (5)$$

When the eigenvalues of the covariance matrix are arranged in descending order, their corresponding eigenvectors  $(\mu_0, \mu_1, \dots, \mu_{p-1})$  are also relatively ordered, and then the features obtained from the projection of the image target on them are also naturally ordered. Therefore, the quantum superposition principle in quantum theory can be used for all the features generated by the image target to prepare a quantum superposition state, as shown below:

$$\frac{1}{\sqrt{p}} \sum_{i=0}^{p-1} \left( \cos \theta_i^j |0\rangle + \sin \theta_i^j |1\rangle \right) |i\rangle \quad \theta_i^j \in [0, \pi] \quad (6)$$

For a recognition image all features need only  $\lceil \log p \rceil + 1$  quantum bits to be represented. Assuming that the number of features per image target is  $p = 8$ , then only four quantum bits are needed to represent these features using quantum bits, while 64 classical bits are needed to represent them using classical bits. This shows that the efficiency of the quantum state is very impressive.

The image features are quantum encoded, then the quantum superposition state of all features of each image can be obtained by H-gate transformation. For the convenience of representation, let:

$$|\hat{\theta}\rangle = \frac{1}{\sqrt{p}} \sum_{i=0}^{p-1} |i\rangle |\text{code}_i\rangle \quad (7)$$

where  $|\text{code}_i\rangle = \cos \theta_i^j |0\rangle + \sin \theta_i^j |1\rangle$ .

Finally, the quantum features of all the image targets in the training set are superimposed to construct the quantum image feature database, so that all the image features in the training set are stored in the quantum image feature database in the form of quantum global feature superposition states, and when the subsequent quantum image classification recognition is carried out, only the quantum features of the image to be recognized need to be compared with the features in the quantum image feature database for similarity. The image can be classified and recognized.

## 2.2 | The INCQI quantum image representation

The INCQI model is mainly proposed to address the problem that the NCQI model cannot handle images with inconsistent horizontal and vertical position sizes and subsequent

transform operations of quantum images [29]. The INCQI model is defined as:

$$|I\rangle = \frac{1}{2^{\frac{n_1+n_2}{2}}} \sum_{y=0}^{2^{n_1}-1} \sum_{x=0}^{2^{n_2}-1} |c(y, x)\rangle \otimes |yx\rangle, \quad (8)$$

where

$$|c(y, x)\rangle = \underbrace{|R_{q-1} \cdots R_0\rangle}_{\text{Red}} \underbrace{|G_{q-1} \cdots G_0\rangle}_{\text{Green}} \underbrace{|B_{q-1} \cdots B_0\rangle}_{\text{Blue}} \underbrace{|\alpha_{q-1} \cdots \alpha_0\rangle}_{\alpha}. \quad (9)$$

$c(y, x)$  denotes the pixel value at position  $(y, x)$ ,  $x$  is the horizontal position, and  $y$  is the vertical position. In addition,  $\alpha$  is an accessory quantum bit to store the intermediate value of each pixel after transformation, such as the threshold value in image segmentation. Compared with NCQI, INCQI contains four channels, three of which are red, green and blue colour channels, and the remaining one is  $\alpha$  calculation channel, which can save pixel calculation results. The range of these four channels is all  $[0, 2^q - 1]$ . For example, for images in the pixel range of 0–255,  $q = 8$ . In addition,  $|yx\rangle$  is expanded according to the binary sequence in the form shown below:

$$|yx\rangle = |y\rangle|x\rangle = |y_0y_1 \dots y_{n_1-1}\rangle |x_0x_1 \dots x_{n_2-1}\rangle \quad (10)$$

In Equation (10),  $y_i, x_i \in \{0, 1\}$ ;  $y, x$  denote the  $Y$ -axis and  $X$ -axis, respectively.

From the definition of INCQI,  $n_1 + n_2 + 4q$  quantum bits are required to store a color image of size  $2^{n_1} \times 2^{n_2}$  using INCQI expressions. A part of quantum image features in the PSQIFE dual quantum image feature extraction method proposed in this paper is mainly based on INCQI quantum images for processing.

### 2.3 | Quantum multi-body state decomposition and quantum feature extraction

The classical image encoded into a quantum image essentially becomes a quantum many-body pure state system, which can be represented as a Matrix Product State (MPS). The Hilbert space of quantum many-body states can be expressed as a series of tensor products of Hilbert spaces:  $\mathcal{H} = \mathcal{H}_1 \otimes \mathcal{H}_2 \otimes \cdots \otimes \mathcal{H}_N$ . For the quantum many-body state  $|\psi\rangle = \sum_{i_1, \dots, i_N=1}^d C_{i_1, \dots, i_N} |i_1, \dots, i_N\rangle$ , its corresponding MPS is expressed as:

$$|\psi\rangle = \sum_{i_1, \dots, i_N=1}^d M_{i_1}^{[1]} M_{i_2}^{[2]} \cdots M_{i_N}^{[N]} |i_1, \dots, i_N\rangle, \quad (11)$$

where  $C_{i_1, \dots, i_N}$  is an  $N$ th order tensor, which is a coefficient containing  $N$  indicators;  $M_{i_1}^{[1]}$  and  $M_{i_N}^{[N]}$  are row and column

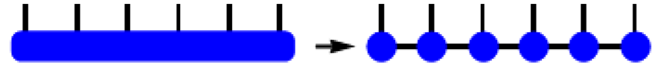


FIGURE 1 The geometric decomposition of MPS

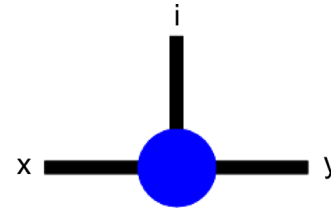


FIGURE 2 The third order tensor

vectors, respectively, multiplied to a number. The geometric decomposition of MPS is shown below (see Figure 1).

An arbitrary finite-dimensional  $N$ th-order tensor can be expressed as the product of  $N$  matrices with indicators, where the coefficients are transformed into a combination of multiple third-order tensors (see Figure 2) by a series of reduction and decomposition of the indicators.

A dense full-rank matrix can be represented as a combination of several low-rank matrices, and the low-rank matrices can be decomposed into products of small-scale matrices. The current advanced low-rank decomposition algorithms mainly include CP decomposition, Tucker decomposition, Tensor Train decomposition and Block Term decomposition, all of which belong to tensor decomposition. Tensor decomposition is a generalization of matrix singular value decomposition as it can maintain the maximum feature of variance contribution in the data set while reducing the dimensionality of the data. Tucker decomposition is also called High Order Singular Value Decomposition (HOSVD), and SVD decomposition is a special form of Tucker decomposition at second order tensor. The tensor low-rank decomposition algorithm of MPS can be used to perform feature extraction of quantum many-body states and realize the low-rank approximation of quantum many-bodies.

### 2.4 | Schmidt decomposition

The Schmidt decomposition is a very important tool in composite quantum systems. For a composite system  $AB$ , the Schmidt decomposition can be stated in the form of the following theorem:

**Theorem 1.** Let  $|\psi\rangle$  be a pure state complex system of the form  $AB$ , then there exist standard orthogonal bases  $|i_A\rangle$  and  $|i_B\rangle$  under system  $A$  and system  $B$ , respectively, such that:

$$|\psi\rangle = \sum_i \lambda_i |i_A\rangle |i_B\rangle \quad (12)$$

where  $\lambda_i \geq 0$  and satisfies  $\sum_i \lambda_i^2 = 1$ , is called the Schmidt coefficient.

**TABLE 3** Schmidt decomposition

---

|   |
|---|
| Input: a composite quantum system $ \psi\rangle$ .  |
| Output: the Schmidt decomposition form of $ \psi\rangle$ .  |
| Step1: Construct the density matrix $\rho =  \psi\rangle\langle\psi $ of the composite system $ \psi\rangle$ .                          |
| Step2: Calculate the approximate density matrices $\rho^A, \rho^B$ for subsystems A and B.  |
| Step3: Calculate the eigenvalues and eigenvectors of $\rho^A$ and $\rho^B$ .  |
| Step4: Construct the Schmidt decomposition form of $ \psi\rangle$ , and get $ \psi\rangle = \sum_i \lambda_i  i_A\rangle  i_B\rangle$ . |

---

*Proof:* Let  $|j\rangle$  and  $|k\rangle$  be a set of standard orthogonal bases belonging to system A and system B, respectively, then the composite system  $|\psi\rangle$  can be written as:

$$|\psi\rangle = \sum_{jk} a_{jk} |j\rangle |k\rangle \quad (13)$$

where the coefficients  $a_{jk}$  form the complex matrix  $a$ , according to the SVD decomposition,  $a = u d v$ , where  $d$  is a diagonal matrix with non-negative elements (if  $j \neq k$ ,  $d$  are diagonal matrices), and  $u$  and  $v$  are You matrices. Then we can obtain:

$$|\psi\rangle = \sum_{jik} u_{ji} d_{ii} v_{ik} |j\rangle |k\rangle \quad (14)$$

Let  $|i_A\rangle \equiv \sum_j u_{ji} |j\rangle$ ,  $|i_B\rangle \equiv \sum_k v_{ik} |k\rangle$ ,  $\lambda_i \equiv d_{ii}$ , we can obtain:

$$|\psi\rangle = \sum_i \lambda_i |i_A\rangle |i_B\rangle \quad (15)$$

Since  $u$  and  $v$  are unitary matrices and  $|j\rangle$  and  $|k\rangle$  are standard orthogonal bases,  $|i_A\rangle$  and  $|i_B\rangle$  form a new set of standard orthogonal bases, respectively.

$|i_A\rangle$  and  $|i_B\rangle$  are called the Schmidt bases of subsystems A and B, respectively, where the number of nonzero  $\lambda_i$  is called the Schmidt coefficient of the composite system  $|\psi\rangle$ , representing the maximum amount of entanglement between subsystems A and B.

In a traditional Schmidt decomposition, the general process is as follows (see Table 3).

This Schmidt decomposition process is very tedious. Here, we adopt the SVD-Schmidt decomposition method to quickly perform the Schmidt decomposition of composite quantum systems by means of the SVD decomposition of matrices. The specific operation procedure is illustrated using an example. Suppose the composite quantum system is:

$$\begin{aligned} |\psi\rangle = & a_0|000\rangle + a_1|001\rangle + a_2|010\rangle + a_3|011\rangle \\ & + a_4|100\rangle + a_5|101\rangle + a_6|110\rangle + a_7|111\rangle. \end{aligned}$$

This is a composite system of three quanta. Let the first quanta be subsystem A and the second and third quanta be

subsystem B. First, write  $(a_0, a_1, a_2, a_3, a_4, a_5, a_6, a_7)^T$  as the following matrix.

$$M = \begin{pmatrix} a_0 & a_1 & a_2 & a_3 \\ a_4 & a_5 & a_6 & a_7 \end{pmatrix} \quad (16)$$

This is a matrix of size  $2 \times 4$ , decomposed by SVD into the standard form  $M = U A V$ , where U is the unitary matrix of size  $2 \times 2$ , V is the unitary matrix of size  $4 \times 4$ , and A is the diagonal matrix of size  $2 \times 4$ . This is shown below:

$$\begin{aligned} & \begin{pmatrix} a_0 & a_1 & a_2 & a_3 \\ a_4 & a_5 & a_6 & a_7 \end{pmatrix} \\ & = \begin{pmatrix} u_0 & u_1 \\ u_2 & u_3 \end{pmatrix} \begin{pmatrix} \lambda_1 & 0 \\ 0 & \lambda_2 \end{pmatrix} \begin{pmatrix} v_0 & v_1 & v_2 & v_3 \\ v_4 & v_5 & v_6 & v_7 \end{pmatrix} = U A V \end{aligned} \quad (17)$$

Based on the above SVD decomposition, we can write the Schmitt decomposition form of the composite system  $|\psi\rangle$  as follows:

$$\begin{aligned} |\psi\rangle = & \lambda_1 \begin{pmatrix} u_0 \\ u_2 \end{pmatrix} \begin{pmatrix} v_0 \\ v_1 \\ v_2 \\ v_3 \end{pmatrix} + \lambda_2 \begin{pmatrix} u_1 \\ u_3 \end{pmatrix} \begin{pmatrix} v_4 \\ v_5 \\ v_6 \\ v_7 \end{pmatrix} \\ = & \lambda_1 |i_{A1}\rangle |i_{B1}\rangle + \lambda_2 |i_{A2}\rangle |i_{B2}\rangle \end{aligned} \quad (18)$$

### 3 | DUAL QUANTUM IMAGE FEATURE EXTRACTION METHOD: PSQIFE

In the process of quantum image classification and recognition, quantum image features can often be used as important credentials for category differentiation. An excellent quantum image feature extraction algorithm can achieve the requirements of classification recognition with the smallest features and the fastest speed. In order to improve the effect and speed of feature extraction, this paper selects the PCA coefficients as the quantum feature encoding of images by analyzing the statistical-based feature extraction methods in classical images, and constructs the quantum image feature extraction method PSQIFE algorithm by combining the SVD-Schmidt decomposition technique. Combining PCA quantum feature encoding and SVD-Schmidt decomposition method, the PSQIFE quantum image feature extraction method is constructed here. The whole PSQIFE quantum image feature extraction method flow is shown as follows (see Figure 3).

#### 3.1 | Construction of the dual quantum image features

In the whole PSQIFE quantum image feature extraction method, it mainly contains the construction of two parts of



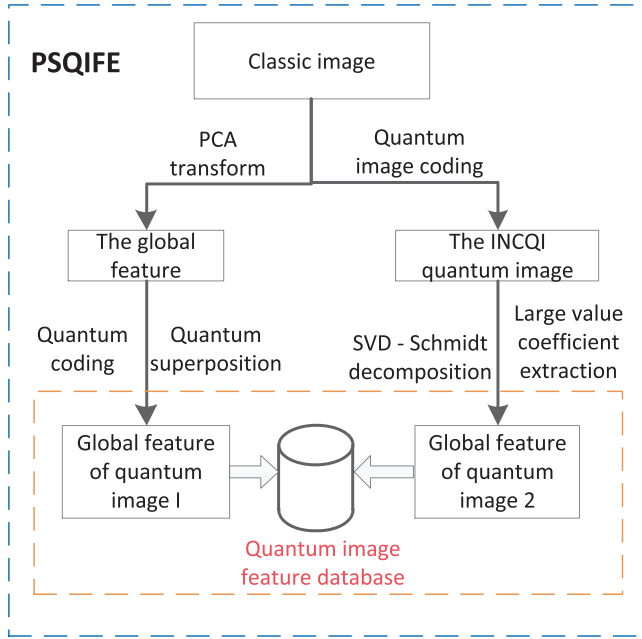


**FIGURE 3** The flow-chart of PSQIFE quantum image feature extraction method

quantum image global features extraction, one part of which is derived from the quantum state encoding composition of features after classical PCA feature extraction of the target image, denoted as  $|F_1\rangle$ . From the previous sections, it is known that after each classical image is encoded into quantum states after PCA, the quantum superposition states of all features are:  $|\hat{\theta}_j\rangle = \frac{1}{\sqrt{p}} \sum_{i=0}^{p-1} |i\rangle |\text{code}_i\rangle$ , where  $j \in \{1, 2, \dots, M\}$ ,  $|\text{code}_i\rangle = \cos \theta_i^j |0\rangle + \sin \theta_i^j |1\rangle$ . Then the quantum features of  $M$  images in the training set can be superimposed to obtain the quantum image features after quantum PCA of classical images:  $|F_1\rangle = \frac{1}{\sqrt{M}} \sum_{j=1}^M |j\rangle \frac{1}{\sqrt{p}} \sum_{i=0}^{p-1} |i\rangle |\text{code}_i\rangle$ , where  $|\text{code}_i\rangle = \cos \theta_i^j |0\rangle + \sin \theta_i^j |1\rangle$ .

For another part of feature acquisition, we mainly constructed by based on INCQI quantum images as well as SVD-Schmidt decomposition. In PSQIFE quantum image feature extraction we extracted INCQI quantum image global features by transforming the training images into INCQI quantum images, and the form of each INCQI quantum image can be written as  $|I\rangle = \frac{1}{2^{\frac{n_1+n_2}{2}}} \sum_{y=0}^{2^{n_1}-1} \sum_{x=0}^{2^{n_2}-1} |c(y, x)\rangle \otimes |yx\rangle$ , where  $|c(y, x)\rangle = |\underbrace{R_{q-1} \dots R_0}_{\text{Red}} \underbrace{G_{q-1} \dots G_0}_{\text{Green}} \underbrace{B_{q-1} \dots B_0}_{\text{Blue}} \underbrace{\alpha_{q-1} \dots \alpha_0}_{\alpha}\rangle$  and  $|yx\rangle = |y\rangle |x\rangle = |y_0 y_1 \dots y_{n_1-1}\rangle |x_0 x_1 \dots x_{n_2-1}\rangle$ .

For the training set  $M$  images into INCQI quantum images after transformation, the large-value coefficients are obtained by SVD-Schmidt decomposition, and then the appropriate number of large-value coefficients is selected, and the projection operator  $\sum_{i \in \{\lambda_i \geq \lambda_k\}} |\Phi_i\rangle \langle \Phi_i|$  is constructed according to the bases corresponding to these large-value coefficients, and the INCQI quantum image global features  $|F_2^k\rangle =$

**TABLE 4** The flow of the PSQIFE method

Input: The image set  $X = (x_1, x_2, \dots, x_K)$ .

Output: The dual-quantum global features  $|F\rangle$

Step 1: Get the classical feature  $\cos(\theta_i^j) = \frac{\mu_i^T d_j}{\sqrt{\lambda_0}}$ ,  $\theta_i^j \in [0, \pi)$  by the process of PCA.

Step 2: Get the quantum feature  $|\text{code}_i\rangle = \cos \theta_i^j |0\rangle + \sin \theta_i^j |1\rangle$  by feature coding.

Step 3: Calculate the quantum image feature  $|\hat{\theta}\rangle$  corresponding to a single classical image by  $|\hat{\theta}\rangle = \frac{1}{\sqrt{p}} \sum_{i=0}^{p-1} |i\rangle |\text{code}_i\rangle$ .

Step 4: Get the quantum image features  $|F_1\rangle$  after quantum PCA of classical images by  $|F_1\rangle = \frac{1}{\sqrt{M}} \sum_{j=1}^M |j\rangle \frac{1}{\sqrt{p}} \sum_{i=0}^{p-1} |i\rangle |\text{code}_i\rangle$ .

Step 5: Get the decomposition form  $|\text{image}\rangle = \sum_{\alpha_1} \sum_{\alpha_2} \dots \sum_{\alpha_{q-1}} \lambda_{\alpha_1} \lambda_{\alpha_2} \dots \lambda_{\alpha_{q-1}} |\Phi_{\alpha_1 \alpha_2 \dots \alpha_{q-1}}\rangle$  of INCQI quantum image corresponding to classical image by SVD-Schmidt decomposition.

Step 6: Get Global feature  $|F_2^k\rangle$  of INCQI quantum image by  $|F_2^k\rangle = \sum_{i \in \{\lambda_i \geq \lambda_k\}} |\Phi_i\rangle \langle \Phi_i| |I_k\rangle$ .

Step 7: Get the global feature superposition state  $|F_2\rangle$  of INCQI quantum image corresponding to the whole image set by

$$|F_2\rangle = \frac{1}{\sqrt{M}} \sum_{j=1}^M |j\rangle \sum_{i \in \{\lambda_i \geq \lambda_k\}} |\Phi_i\rangle \langle \Phi_i| |I_k\rangle.$$

Step 8: Get the dual-quantum global features  $|F\rangle$  of whole image set by  $|F\rangle = |F_1\rangle \otimes |F_2\rangle$

$\sum_{i \in \{\lambda_i \geq \lambda_k\}} |\Phi_i\rangle \langle \Phi_i| |I_k\rangle$  are extracted on the INCQI quantum image using the projection operator action, where  $k \in \{1, 2, \dots, M\}$ . Then the quantum image global features of the total  $M$  INCQI quantum images can be superimposed to obtain  $|F_2\rangle = \frac{1}{\sqrt{M}} \sum_{j=1}^M |j\rangle \sum_{i \in \{\lambda_i \geq \lambda_k\}} |\Phi_i\rangle \langle \Phi_i| |I_k\rangle$ .

In total, two different quantum global features of A and B are obtained, one from the classical image feature extraction after quantum feature encoding, and one is the quantum image global feature obtained by quantum feature extraction after the classical image is transformed into INCQI quantum image, so that the two quantum global features constitute a dual quantum global feature.  $|F\rangle = |F_1\rangle \otimes |F_2\rangle$  is obtained by merging  $|F_1\rangle$  and  $|F_2\rangle$ . These dual-quantum global features  $|F\rangle$  constitute a quantum image feature library. The flow of the PSQIFE is as follows (see Table 4).

There are many models of quantum image representation, but no matter which quantum image format is used, it is a pure state system with multiple quantum bits. For a classical image of size  $2^n \times 2^n$ , it becomes a pure state composite system of  $2n$  quantum bits after quantum image encoding. This is shown as:

$$|\text{image}\rangle = \sum_{j_1=0}^1 \sum_{j_2=0}^1 \dots \sum_{j_n=0}^1 C_{j_1 j_2 \dots j_n} |j_1\rangle \otimes |j_2\rangle \otimes \dots \otimes |j_n\rangle \quad (19)$$

where  $C_{j_1 j_2 \dots j_n}$  represents the greyscale value at the  $|j_1 j_2 \dots j_n\rangle$  coordinate.

According to the SVD-Schmidt decomposition method, we may take the 1st quantum bit as subsystem A and the remaining  $n - 1$  quantum bits  $|j_2\rangle \otimes \dots \otimes |j_n\rangle$  as subsystem B. After decomposition, we can get:

$$|\text{image}\rangle = \sum_{\alpha_1} \lambda_{\alpha_1} |\Phi_{\alpha_1}\rangle |\Phi_{\alpha_1}^{[2\dots n]}\rangle \quad (20)$$

where  $\alpha_1$  represents the first decomposition of  $|\text{image}\rangle$ , and the decompositions obtained  $|\Phi_{\alpha_1}\rangle$  and  $|\Phi_{\alpha_1}^{[2\dots n]}\rangle$  represent the Schmidt bases of subsystems A and B, respectively.

Following the same decomposition method,  $|\Phi_{\alpha_1}^{[2\dots n]}\rangle$  is decomposed in turn until a subsystem consisting of all single quantum bits is obtained. This is shown as:

$$|\text{image}\rangle = \sum_{\alpha_1} \sum_{\alpha_2} \dots \sum_{\alpha_{n-1}} \lambda_{\alpha_1} \lambda_{\alpha_2} \dots \lambda_{\alpha_{n-1}} |\Phi_{\alpha_1 \alpha_2 \dots \alpha_{n-1}}\rangle \quad (21)$$

In this way, we obtain the representation of the quantum image under another set of Schmidt bases. This form is similar to performing Fourier transform, wavelet transform, etc. on a classical image, where the majority of coefficients are equal to 0 or close to 0. The main energy of the image is concentrated in a few large-valued coefficients, which can be considered as the global features of the quantum image.

### 3.2 | The introduction of evaluation indicators

Similar to classical image feature extraction algorithms, it is important to evaluate the effectiveness of quantum image feature extraction methods. Here, we focus on the evaluation of both the fidelity of quantum images and the effectiveness of quantum image features for image classification.

#### 3.2.1 | The fidelity of quantum images

The fidelity of the reconstructed quantum image varies with the choice of different large-value coefficients. The fidelity is a common metric that can be used to measure the distance between two quantum states, which is defined in the form of the modulus  $|\langle\psi|\psi\rangle|$  of the inner product of two quantum states. the closer this value is to 1, the closer the two quantum states are. To measure the quality of the recovered image, it is described by an approximation of the fidelity, defined as shown below.

$$\text{fidelity} = \sum_{\{\text{the largest } k \text{ coefficients}\}} |\lambda_k|^2 \quad (22)$$

After the quantum image is decomposed by SVD-Schmidt, the energy of the image is mainly retained in a small number of large-valued coefficients, which represent the global features of the quantum image and can be used to represent and approximate the original image.

#### 3.2.2 | The effectiveness of quantum image features for image classification accuracy

In this paper, we mainly use PSQIFE quantum image feature extraction method and convolutional neural network (CNN) feature extraction method on the Mnist dataset [30] to compare the classification effect.

## 4 | EXPERIMENT

In this section, in order to validate the PSQIFE quantum image feature extraction method, we perform quantum image reconstruction by extracting the global features of the quantum image and test the fidelity of the reconstructed quantum image. In addition, the classification accuracy of image features obtained by different feature extraction methods on Mnist dataset [30] is compared with the CNN method to determine the effectiveness of the feature extraction methods. The experimental tests in this paper were performed on the IBM Quantum Cloud platform (IBMQ) [31], where Matlab software was also used for some of the image data processing.

### 4.1 | The experimental images

In order to test that the PSQIFE quantum image feature extraction method has better results for images with different feature distributions, we have chosen some classical digitally processed images for our experiments. The details are shown below (see Figure 4).

These images are all grey images of size 512×512, and their histogram distribution is shown in Figure 5.

As can be seen from the histogram distribution above, the images used in the experiments are relatively evenly distributed, except for “Saturn.jpg”, which has a more concentrated pixel distribution. These classical digital images were chosen because they represent problems that are more difficult for image reconstruction algorithms to deal with, such as reproducing details and textures, strong variations and edges, and balanced regions. Therefore, these images are chosen to test the effectiveness of the PSQIFE quantum image feature extraction method and are representative.

### 4.2 | The experimental and result analysis

In order to validate the PSQIFE quantum image feature extraction method, this paper conducts experiments on the nine classical digital images selected above. According to the PSQIFE quantum image feature extraction process, we convert these classical digital images into quantum images in the INCQI format. For an INCQI quantum image of size  $2^N \times 2^N$ , a total of  $2N + 4q$  quantum bits are required when 4-channel encoding is performed, where  $q$  is the colour depth, and  $q = 8$  for images with colour values of 0–255. Here, we perform quantum image reconstruction on the extracted global features of

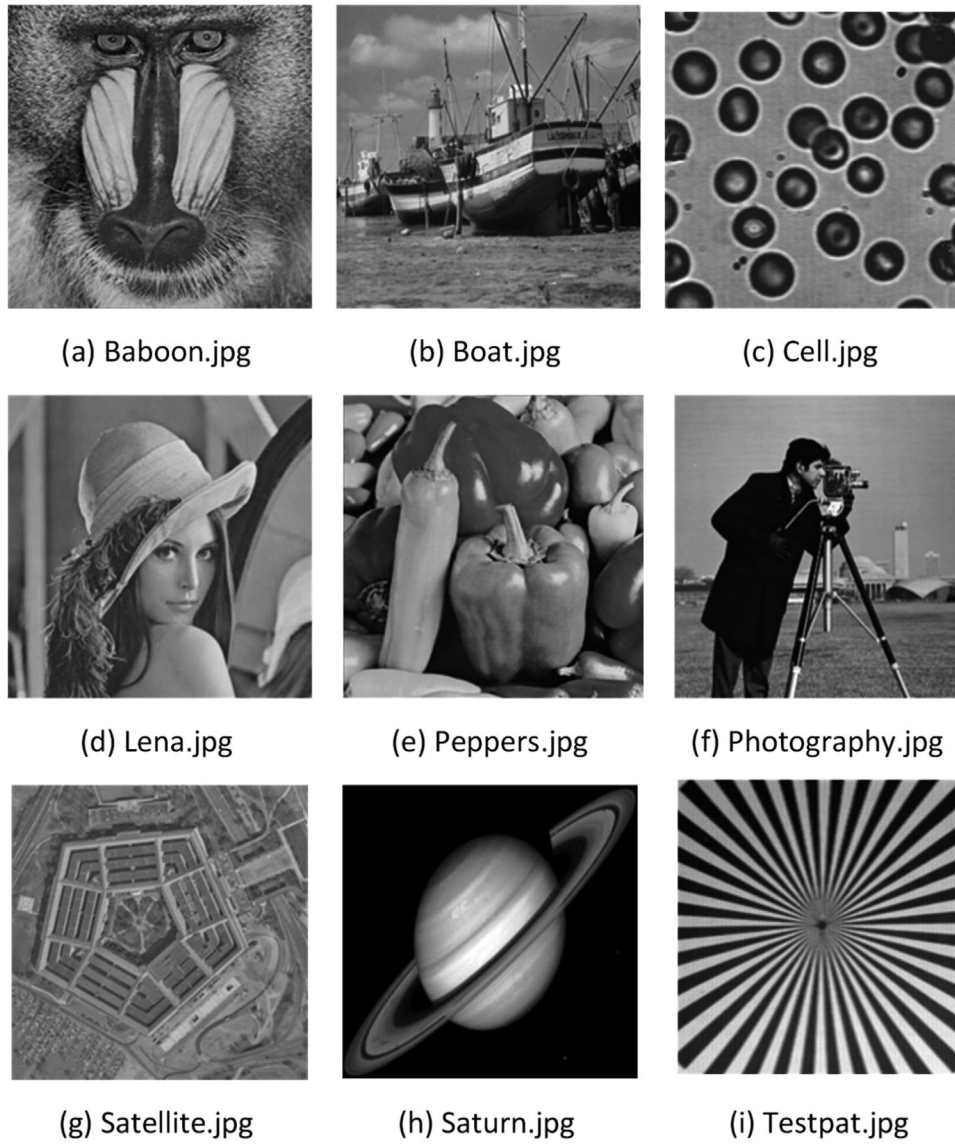


FIGURE 4 The experimental images

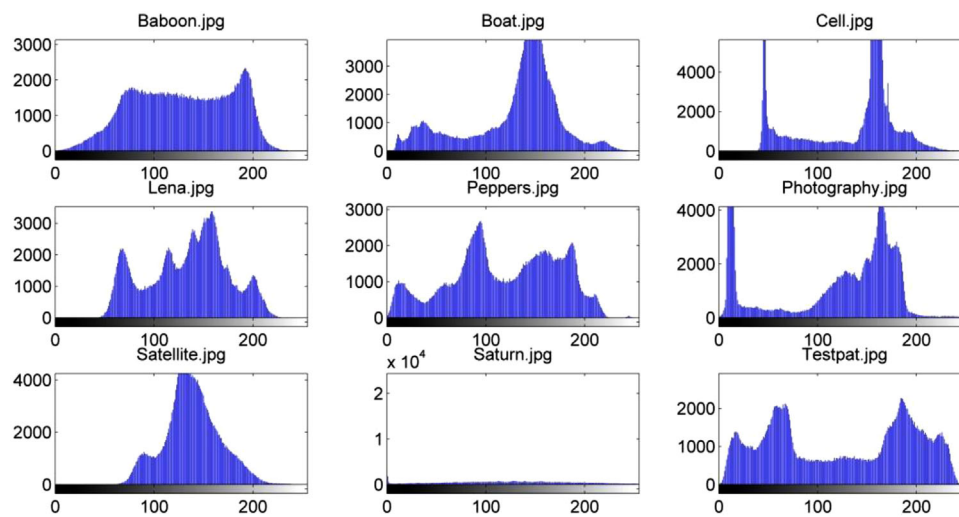


FIGURE 5 The histogram of the experimental image



**TABLE 5** Distribution of INCQI quantum image codes corresponding to size  $512 \times 512$  greyscale images

| Location      | $ 0\rangle$         | $ 1\rangle$         | $ j\rangle$ | $ 511\rangle$         |
|---------------|---------------------|---------------------|-------------|-----------------------|
| $ 0\rangle$   | $ C_{0,0}\rangle$   | $ C_{0,1}\rangle$   | ...         | $ C_{0,511}\rangle$   |
| $ 1\rangle$   | $ C_{1,0}\rangle$   | $ C_{1,1}\rangle$   | ...         | $ C_{1,511}\rangle$   |
| $ i\rangle$   | ...                 | ...                 | ...         | ...                   |
| $ 511\rangle$ | $ C_{511,0}\rangle$ | $ C_{511,1}\rangle$ | ...         | $ C_{511,511}\rangle$ |

quantum images and test the fidelity of the reconstructed quantum images. The above classical digital images are all grayscale images of size  $512 \times 512$ , and the number of quantum bits required to convert them into INCQI quantum images is  $2 \times 9 + 4 \times 8 = 50$ . In order to reduce the complexity of the experiment, only a single channel is used for the grayscale image, so the number of quantum bits required is reduced to  $2 \times 9 + 8 = 26$ . For an INCQI quantum image composed of 26 quantum bits, which is in fact a multi-body quantum pure state system, the global features of the quantum image are extracted and decomposed by SVD-Schmidt, and finally decomposed into a subsystem composed of all single quantum subsystem composed of bits, a total of 25 decompositions are needed to obtain  $2^{25}$  Schmidt coefficients.

The pixel values of the selected classical images are expanded into a column vector in the order of top to bottom and left to right, respectively, and normalized. These vectors correspond to the INCQI quantum image. The INCQI quantum image can then be viewed as a composite quantum system, which is decomposed into a subsystem composed of single quantum bits by the decomposition method in the PSQIFE quantum image feature extraction method introduced earlier. After getting all the Schmidt coefficients, the INCQI quantum image is reconstructed by picking different numbers of coefficients, and after that the fidelity between the reconstructed image and the original image is compared. For a grayscale image of size  $512 \times 512$ , the INCQI quantum image is used to represent the corresponding position and colour coding distribution as shown below (see Table 5).

This greyscale image corresponds to the INCQI quantum image of the form:

$$|\text{Image}\rangle = \frac{1}{2^9} \sum_{y=0}^{501} \sum_{x=0}^{501} |C(y, x)\rangle \otimes |yx\rangle. \quad (23)$$

It is an INCQI quantum image consisting of 26 quantum bits, which is obviously a quantum many-body pure state system with 26 quantum bits and can be written in the following form:

$$|\text{Image}\rangle = \frac{1}{2^9} \sum_{j_1=0}^1 \sum_{j_2=0}^1 \dots \sum_{j_n=0}^1 |C_{j_1 j_2 \dots j_n}\rangle |j_1\rangle \otimes |j_2\rangle \otimes \dots \otimes |j_n\rangle \quad (24)$$

where  $n = 2 * 9 = 18$ , and since the colour depth of the grayscale image is  $q = 8$ ,  $|C_{j_1 j_2 \dots j_n}\rangle$  is a quantum state consist-

ing of 8 quantum bits in the range  $[0, 2^q - 1]$ . It can be written in the form of a single quantum bit, as follows:

$$|C_{j_1 j_2 \dots j_n}\rangle = |C_{j_1 j_2 \dots j_n}^0\rangle \otimes |C_{j_1 j_2 \dots j_n}^1\rangle \dots \otimes |C_{j_1 j_2 \dots j_n}^7\rangle \quad (25)$$

where  $|C_{j_1 j_2 \dots j_n}^k\rangle \in \{0, 1\}$ . Combining the above equation, the INCQI quantum image corresponding to a grayscale image of size  $512 \times 512$  can be obtained expressed in the form of a single quantum bit as:

$$|\text{Image}\rangle = \frac{1}{2^9} \sum_{j_1=0}^1 \sum_{j_2=0}^1 \dots \sum_{j_n=0}^1 |C_{j_1 j_2 \dots j_n}^0\rangle \otimes |C_{j_1 j_2 \dots j_n}^1\rangle \dots \otimes |C_{j_1 j_2 \dots j_n}^7\rangle |j_1\rangle \otimes |j_2\rangle \otimes \dots \otimes |j_n\rangle \quad (26)$$

First, choosing the 1st quantum bit  $|C_{j_1 j_2 \dots j_n}^0\rangle$  as subsystem A and the remaining 25 quantum bits as subsystem B, the SVD-Schmidt decomposition can be obtained in the following form:

$$|\text{Image}\rangle = \frac{1}{2^9} \sum_{\alpha_1} \lambda_{\alpha_1} |\Phi_{\alpha_1}\rangle |\Phi_{\alpha_1}^{[2\dots 25]}\rangle \quad (27)$$

where  $\alpha_1$  denotes the 1st decomposition,  $|\Phi_{\alpha_1}\rangle$  and  $|\Phi_{\alpha_1}^{[2\dots 25]}\rangle$  denote the Schmidt bases of subsystems A and B. Then the 2nd decomposition of  $|\Phi_{\alpha_1}^{[2\dots 25]}\rangle$  is performed to obtain the 2nd quantum bit and the subsystem consisting of the remaining 24 quantum bits, at which time the corresponding INCQI quantum image can be written and expressed in the following form:

$$|\text{Image}\rangle = \frac{1}{2^9} \sum_{\alpha_1} \lambda_{\alpha_1} |\Phi_{\alpha_1}\rangle |\Phi_{\alpha_1}^{[2\dots 25]}\rangle \left( \sum_{\alpha_2} \lambda_{\alpha_2} |\Phi_{\alpha_2}\rangle |\Phi_{\alpha_2}^{[3\dots 25]}\rangle \right) \quad (28)$$

Following the same method of sequential decomposition, a subsystem composed entirely of single quantum bits is obtained:

$$|\text{Image}\rangle = \frac{1}{2^9} \sum_{\alpha_1} \sum_{\alpha_2} \dots \sum_{\alpha_{n-1}} \lambda_{\alpha_1} \lambda_{\alpha_2} \dots \lambda_{\alpha_{n-1}} |\Phi_{\alpha_1 \alpha_2 \dots \alpha_{n-1}}\rangle \quad (29)$$

This yields a subsystem formed by the SVD-Schmidt decomposition of the INCQI quantum image corresponding to a grayscale image of size  $512 \times 512$ . The flow of the whole decomposition process can be represented in the form of a tensor network as follows [32–34].

In the above decomposition (see Figure 6), 1 multi-quantum bit system consisting of 26 quantum bits undergoes 25 rounds of decomposition, resulting in a subsystem of 26 single quantum bits.

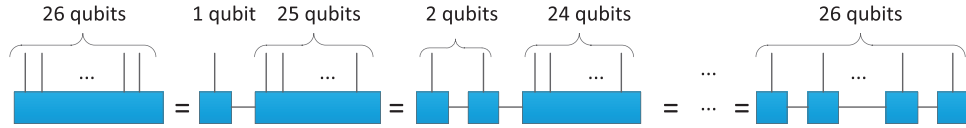


FIGURE 6 The flow chart of SVD-Schmidt decomposition

| 512x512 uint8 |     |     |     |     |     |     |     |     |     |     |     |     |     |
|---------------|-----|-----|-----|-----|-----|-----|-----|-----|-----|-----|-----|-----|-----|
|               | 501 | 502 | 503 | 504 | 505 | 506 | 507 | 508 | 509 | 510 | 511 | 512 |     |
| 496           | 63  | 59  | 58  | 61  | 61  | 62  | 62  | 56  | 52  | 53  | 65  | 54  |     |
| 497           | 60  | 52  | 60  | 60  | 63  | 65  | 62  | 53  | 58  | 55  | 59  | 47  |     |
| 498           | 64  | 61  | 59  | 55  | 63  | 58  | 54  | 51  | 51  | 55  | 55  | 53  |     |
| 499           | 59  | 62  | 61  | 56  | 54  | 53  | 49  | 53  | 56  | 52  | 55  | 42  | 41  |
| 500           | 60  | 54  | 56  | 60  | 55  | 49  | 50  | 49  | 40  | 48  | 51  | 58  |     |
| 501           | 61  | 55  | 57  | 63  | 56  | 50  | 55  | 55  | 56  | 52  | 52  | 53  | 48  |
| 502           | 59  | 54  | 60  | 61  | 50  | 53  | 56  | 51  | 54  | 55  | 59  | 67  | 64  |
| 503           | 61  | 54  | 57  | 54  | 53  | 54  | 58  | 57  | 61  | 50  | 56  | 68  | 83  |
| 504           | 60  | 69  | 66  | 50  | 56  | 49  | 45  | 48  | 63  | 58  | 72  | 74  | 91  |
| 505           | 55  | 59  | 56  | 59  | 76  | 55  | 50  | 62  | 71  | 74  | 70  | 79  | 84  |
| 506           | 51  | 53  | 56  | 51  | 70  | 58  | 60  | 67  | 73  | 84  | 82  | 89  | 98  |
| 507           | 55  | 54  | 58  | 66  | 63  | 56  | 68  | 75  | 80  | 94  | 91  | 87  | 93  |
| 508           | 56  | 55  | 55  | 57  | 66  | 67  | 78  | 82  | 85  | 95  | 95  | 91  | 93  |
| 509           | 56  | 57  | 57  | 61  | 70  | 75  | 81  | 88  | 93  | 97  | 100 | 99  | 95  |
| 510           | 50  | 55  | 60  | 73  | 68  | 80  | 82  | 91  | 102 | 99  | 103 | 103 | 97  |
| 511           | 58  | 66  | 72  | 74  | 85  | 94  | 90  | 94  | 103 | 99  | 104 | 107 | 107 |
| 512           | 59  | 68  | 71  | 80  | 82  | 94  | 92  | 94  | 105 | 102 | 104 | 104 | 108 |

FIGURE 7 Partial pixels of “Lena.jpg” image of size 512 × 512

Take “Lena.jpg”, one of the nine images in the experiment, for example, it contains a total of 512×512 pixel values, and the specific pixel values are displayed as shown below (see Figure 7).

After arranging the pixel values into a column vector according to the top to bottom and left to right, and performing L2 parametric normalization, the coefficients of the corresponding quantum image (quantum state) can be defined as  $|\varphi\rangle = [0.0024, 0.0024, \dots, 0.0016, 0.0016]^T_{1 \times 262144}$ . Next, Reshape the normalized column vector to obtain

$$\begin{bmatrix} 0.0024 & 0.0024 & \dots & 0.0014 & 0.0016 \\ 0.0024 & 0.0024 & \dots & 0.0014 & 0.0016 \end{bmatrix}_{2 \times 131072}$$

Following the SVD-Schmidt decomposition process, after the 1st decomposition, the following can be obtained:

$$\begin{aligned} & \begin{bmatrix} 0.0024 & 0.0024 & \dots & 0.0014 & 0.0016 \\ 0.0024 & 0.0024 & \dots & 0.0014 & 0.0016 \end{bmatrix}_{2 \times 131072} \\ &= \begin{bmatrix} -0.7072 & -0.7071 \\ -0.7071 & 0.7072 \end{bmatrix}_{2 \times 2} \times \begin{bmatrix} 0.9995 & 0 \\ 0 & 0.0314 \end{bmatrix}_{2 \times 2} \\ &\times \begin{bmatrix} -0.0034 & -0.0034 & \dots & -0.0020 & -0.0022 \\ -3.2348e-4 & 3.3908e-4 & \dots & 6.6719e-4 & 3.3647e-4 \end{bmatrix}_{2 \times 131072} \end{aligned} \quad (30)$$

At this point, the quantum state  $|\varphi\rangle$  can be defined as follows:

$$\begin{aligned} |\varphi\rangle &= 0.9995 \begin{pmatrix} -0.7072 \\ -0.7071 \end{pmatrix} \begin{pmatrix} -0.0034 \\ -0.0034 \\ \vdots \\ -0.0020 \\ -0.0022 \end{pmatrix}_{131072 \times 1} \\ &+ 0.0314 \begin{pmatrix} -0.7071 \\ 0.7072 \end{pmatrix} \begin{pmatrix} -3.2348e-4 \\ 3.3908e-4 \\ \vdots \\ 6.6719e-4 \\ 3.3647e-4 \end{pmatrix}_{131072 \times 1} \end{aligned} \quad (31)$$

Reshape the vectors

$$|\varphi_{11}\rangle = \begin{pmatrix} -0.0034 \\ -0.0034 \\ \vdots \\ -0.0020 \\ -0.0022 \end{pmatrix}_{131072 \times 1}$$

and

$$|\varphi_{12}\rangle = \begin{pmatrix} -3.2348e-4 \\ 3.3908e-4 \\ \vdots \\ 6.6719e-4 \\ 3.3647e-4 \end{pmatrix}_{131072 \times 1}$$

obtained after the 1st decomposition into  $2 \times 65,536$  matrices to obtain

$$\begin{bmatrix} -0.0034 & -0.0034 & \cdots & -0.0019 & -0.0020 \\ -0.0034 & -0.0033 & \cdots & -0.0019 & -0.0022 \end{bmatrix}_{2 \times 65536}$$

and

$$\begin{bmatrix} -3.2348e-4 & 7.8726e-6 & \cdots & 4.6e-3 & 6.6719e-4 \\ 3.3908e-4 & -6.5478e-4 & \cdots & 4.4917e-6 & 3.3647e-4 \end{bmatrix}_{2 \times 65536},$$

and then carry out the 2nd decomposition in turn, we can obtain:

$$\begin{aligned} & \begin{bmatrix} -0.0034 & -0.0034 & \cdots & -0.0019 & -0.0020 \\ -0.0034 & -0.0033 & \cdots & -0.0019 & -0.0022 \end{bmatrix}_{2 \times 65536} \\ &= \begin{bmatrix} -0.7072 & -0.7070 \\ -0.7070 & 0.7072 \end{bmatrix}_{2 \times 2} \times \begin{bmatrix} 0.9989 & 0 \\ 0 & 0.0464 \end{bmatrix}_{2 \times 2} \quad (32) \\ &\times \begin{bmatrix} 0.0048 & 0.0048 & \cdots & 0.0027 & 0.0030 \\ -1.6333e-5 & 6.1644e-4 & \cdots & -6.4235e-4 & -3.6e-3 \end{bmatrix}_{2 \times 65536} \end{aligned}$$

and

$$\begin{aligned} & \begin{bmatrix} -3.2348e-4 & 7.8726e-6 & \cdots & 4.6e-3 & 6.6719e-4 \\ 3.3908e-4 & -6.5478e-4 & \cdots & 4.4917e-6 & 3.3647e-4 \end{bmatrix}_{2 \times 65536} \\ &= \begin{bmatrix} -0.9980 & 0.0636 \\ 0.0636 & 0.9980 \end{bmatrix}_{2 \times 2} \times \begin{bmatrix} 0.7159 & 0 \\ 0 & 0.6982 \end{bmatrix}_{2 \times 2} \quad (33) \\ &\times \begin{bmatrix} 4.8105e-4 & -6.9164e-5 & \cdots & -6.5e-3 & 4.2947e-4 \\ 4.5520e-4 & -9.3523e-4 & \cdots & -9.0014e-4 & 5.4175e-4 \end{bmatrix}_{2 \times 65536} \end{aligned}$$

At this point, the quantum states  $|\varphi_{11}\rangle$  and  $|\varphi_{12}\rangle$  can be defined as follows:

$$|\varphi_{11}\rangle = 0.9989 \begin{pmatrix} 0.7072 \\ -0.7070 \\ \vdots \\ 0.0027 \\ 0.0030 \end{pmatrix}_{65536 \times 1}$$

$$+ 0.0464 \begin{pmatrix} -0.7070 \\ 0.7072 \end{pmatrix} \begin{pmatrix} -1.6333e-5 \\ 6.1644e-4 \\ \vdots \\ -6.4235e-4 \\ -3.6e-3 \end{pmatrix}_{65536 \times 1} \quad (34)$$

$$|\varphi_{12}\rangle = 0.7159 \begin{pmatrix} -0.9980 \\ 0.0636 \end{pmatrix} \begin{pmatrix} 4.8105e-4 \\ -6.9164e-5 \\ \vdots \\ -6.5e-3 \\ 4.2947e-4 \end{pmatrix}_{65536 \times 1}$$

$$+ 0.6982 \begin{pmatrix} 0.0636 \\ 0.9980 \end{pmatrix} \begin{pmatrix} 4.5520e-4 \\ -9.3523e-4 \\ \vdots \\ -9.0014e-4 \\ 5.4175e-4 \end{pmatrix}_{65536 \times 1} \quad (35)$$

Then the vectors

$$|\varphi_{21}\rangle = \begin{pmatrix} 0.0048 \\ 0.0048 \\ \vdots \\ 0.0027 \\ 0.0030 \end{pmatrix}_{65536 \times 1},$$

$$|\varphi_{22}\rangle = \begin{pmatrix} -1.6333e-5 \\ 6.1644e-4 \\ \vdots \\ -6.4235e-4 \\ -3.6e-3 \end{pmatrix}_{65536 \times 1},$$

$$|\varphi_{23}\rangle = \begin{pmatrix} 4.8105e-4 \\ -6.9164e-5 \\ \vdots \\ -6.5e-3 \\ 4.2947e-4 \end{pmatrix}_{65536 \times 1}$$

and

$$|\varphi_{24}\rangle = \begin{pmatrix} 4.5520e-4 \\ -9.3523e-4 \\ \vdots \\ -9.0014e-4 \\ 5.4175e-4 \end{pmatrix}_{65536 \times 1}$$

obtained after the 2nd decomposition are reshaped into  $2 \times 32768$  matrices to obtain

$$\begin{bmatrix} 0.0048 & 0.0046 & \cdots & 0.0015 & 0.0027 \\ 0.0048 & 0.0046 & \cdots & 0.0021 & 0.0030 \end{bmatrix}_{2 \times 32768},$$

$$\begin{bmatrix} -1.6333e-5 & 1.4246e-4 & \cdots & 1.5331e-4 & -6.4235e-4 \\ 6.1644e-4 & 4.5871e-4 & \cdots & -9.8e-3 & -3.6e-3 \end{bmatrix}_{2 \times 32768},$$

$$\begin{bmatrix} 4.8105e-4 & -1.4e-3 & \cdots & -2.3e-3 & -6.5e-3 \\ -6.9164e-5 & 5.1067e-4 & \cdots & -7.2e-3 & -9.0014e-4 \end{bmatrix}_{2 \times 32768}$$

and

$$\begin{bmatrix} 4.5520e-4 & 1.0195e-4 & \cdots & 8.2e-3 & 4.2947e-4 \\ -9.3523e-4 & 9.2841e-4 & \cdots & 4.3e-3 & 5.4175e-4 \end{bmatrix}_{2 \times 32768}.$$

Then the 3rd decomposition is performed in turn, and the following can be obtained:

$$\begin{bmatrix} 0.0048 & 0.0046 & \cdots & 0.0015 & 0.0027 \\ 0.0048 & 0.0046 & \cdots & 0.0021 & 0.0030 \end{bmatrix}_{2 \times 32768}$$

$$= \begin{bmatrix} -0.7076 & -0.7066 \\ -0.7066 & 0.7076 \end{bmatrix}_{2 \times 2} \times \begin{bmatrix} 0.9980 & 0 \\ 0 & 0.0636 \end{bmatrix}_{2 \times 2} \quad (36)$$

$$\times \begin{bmatrix} -0.0067 & -0.0065 & \cdots & -0.0025 & -0.0040 \\ 2.4181e-4 & 8.9359e-4 & \cdots & 0.0071 & 0.0032 \end{bmatrix}_{2 \times 32768}$$

$$\begin{bmatrix} -1.6333e-5 & 1.4246e-4 & \cdots & 1.5331e-4 & -6.4235e-4 \\ 6.1644e-4 & 4.5871e-4 & \cdots & -9.8e-3 & -3.6e-3 \end{bmatrix}_{2 \times 32768}$$

$$= \begin{bmatrix} -0.6460 & 0.7634 \\ 0.7634 & 0.6460 \end{bmatrix}_{2 \times 2} \times \begin{bmatrix} 0.7548 & 0 \\ 0 & 0.6559 \end{bmatrix}_{2 \times 2} \quad (37)$$

$$\times \begin{bmatrix} 6.3739e-4 & 3.4199e-4 & \cdots & -0.0101 & -0.0031 \\ 5.8808e-4 & 6.1755e-4 & \cdots & -0.0095 & -0.0043 \end{bmatrix}_{2 \times 32768}$$

$$\begin{bmatrix} 4.8105e-4 & -1.4e-3 & \cdots & -2.3e-3 & -6.5e-3 \\ -6.9164e-5 & 5.1067e-4 & \cdots & -7.2e-3 & -9.0014e-4 \end{bmatrix}_{2 \times 32768}$$

$$= \begin{bmatrix} -0.6875 & 0.7262 \\ 0.7262 & 0.6875 \end{bmatrix}_{2 \times 2} \times \begin{bmatrix} 0.7404 & 0 \\ 0 & 0.6722 \end{bmatrix}_{2 \times 2} \quad (38)$$

$$\times \begin{bmatrix} -5.1450e-4 & 0.0018 & \cdots & -0.0049 & 0.0051 \\ 4.4899e-4 & -9.8507e-4 & \cdots & -0.0098 & -0.0079 \end{bmatrix}_{2 \times 32768}$$

$$\begin{bmatrix} 4.5520e-4 & 1.0195e-4 & \cdots & 8.2e-3 & 4.2947e-4 \\ -9.3523e-4 & 9.2841e-4 & \cdots & 4.3e-3 & 5.4175e-4 \end{bmatrix}_{2 \times 32768}$$

$$= \begin{bmatrix} -0.6148 & 0.7887 \\ 0.7887 & 0.6148 \end{bmatrix}_{2 \times 2} \times \begin{bmatrix} 0.7399 & 0 \\ 0 & 0.6728 \end{bmatrix}_{2 \times 2} \quad (39)$$

$$\times \begin{bmatrix} -0.0014 & 9.0498e-4 & \cdots & -0.0023 & 2.2065e-4 \\ -3.2098e-4 & 9.6792e-4 & \cdots & 0.0136 & 9.9854e-4 \end{bmatrix}_{2 \times 32768}$$

At this point, the quantum states  $|\varphi_{21}\rangle$ ,  $|\varphi_{22}\rangle$ ,  $|\varphi_{23}\rangle$  and  $|\varphi_{24}\rangle$  can be defined as follows:

$$|\varphi_{21}\rangle = 0.9980 \begin{pmatrix} -0.7076 \\ -0.7066 \\ \vdots \\ -0.0025 \\ -0.0040 \end{pmatrix}_{32768 \times 1}$$

$$+ 0.0636 \begin{pmatrix} -0.7066 \\ 0.7076 \end{pmatrix} \begin{pmatrix} 2.4181e-4 \\ 8.9359e-4 \\ \vdots \\ 0.0071 \\ 0.0032 \end{pmatrix}_{32768 \times 1} \quad (40)$$

$$|\varphi_{22}\rangle = 0.7548 \begin{pmatrix} -0.6460 \\ 0.7634 \end{pmatrix} \begin{pmatrix} 6.3739e-4 \\ 6.1755e-4 \\ \vdots \\ -0.0101 \\ -0.0031 \end{pmatrix}_{32768 \times 1}$$

$$+ 0.6559 \begin{pmatrix} 0.7634 \\ 0.6460 \end{pmatrix} \begin{pmatrix} 5.8808e-4 \\ 6.1755e-4 \\ \vdots \\ -0.0095 \\ -0.0043 \end{pmatrix}_{32768 \times 1} \quad (41)$$

$$|\varphi_{23}\rangle = 0.7404 \begin{pmatrix} -0.6875 \\ 0.7262 \end{pmatrix} \begin{pmatrix} -5.1450e-4 \\ 0.0018 \\ \vdots \\ -0.0049 \\ 0.0051 \end{pmatrix}_{32768 \times 1}$$

$$+ 0.6722 \begin{pmatrix} 0.7262 \\ 0.6875 \end{pmatrix} \begin{pmatrix} 4.4899e-4 \\ -9.8507e-4 \\ \vdots \\ -0.0098 \\ -0.0079 \end{pmatrix}_{32768 \times 1} \quad (42)$$



**TABLE 6** Comparison of image reconstruction fidelity of Lena images with different numbers of SVD-Schmidt coefficients in the PSQIFE method

| Coefficients selected | Total number of coefficients | Percentage of coefficients selected | Fidelity (%) |
|-----------------------|------------------------------|-------------------------------------|--------------|
| $2^{18}$              | $2^{19}$                     | 50%                                 | 99.95        |
| $2^{17}$              | $2^{19}$                     | 25%                                 | 99.84        |
| $2^{16}$              | $2^{19}$                     | 12.5%                               | 99.64        |
| $2^{15}$              | $2^{19}$                     | 6.25%                               | 99.3         |
| $2^{14}$              | $2^{19}$                     | 3.125%                              | 98.76        |
| $2^{13}$              | $2^{19}$                     | 1.56%                               | 97.98        |
| $2^{12}$              | $2^{19}$                     | 0.78%                               | 96.78        |
| $2^{11}$              | $2^{19}$                     | 0.39%                               | 95.56        |

$$\begin{aligned}
 |\varphi_{24}\rangle = & 0.7399 \begin{pmatrix} -0.6148 \\ 0.7887 \end{pmatrix} \begin{pmatrix} -0.0014 \\ 9.0498e-4 \\ \vdots \\ -0.0023 \\ 2.2065e-4 \end{pmatrix}_{32768 \times 1} \\
 & + 0.6278 \begin{pmatrix} 0.7887 \\ 0.6148 \end{pmatrix} \begin{pmatrix} -3.2098e-4 \\ 9.6792e-4 \\ \vdots \\ 0.0136 \\ 9.9854e-4 \end{pmatrix}_{32768 \times 1} \quad (43)
 \end{aligned}$$

The quantum states obtained after the 3rd decomposition are operated in the same way, and finally, a subsystem composed of all single quantum bits can be obtained.

Eventually, the ‘‘Lena’’ image is decomposed in multiple rounds to obtain all Schmidt coefficients, and the quantum states (quantum images) are reconstructed by picking different numbers of maximum coefficients. The quality of the reconstructed quantum image after the global feature selection of the quantum image is measured by the fidelity. The specific comparison is shown in the following table (see Table 6).

From Table 6, it is known that the feature large value coefficients obtained by the PSQIFE quantum image feature extraction method possess the main energy of the image and can well represent the global features of the image, thus allowing to represent and approximate the original image with. It is effective for the extraction of quantum image features.

For the remaining eight classical images in the experiment the same method is used to test the fidelity that can be derived under different SVD-Schmidt coefficient selections, and finally the fidelity of a total of nine test images (a–i) is compared and the average fidelity (j) is calculated.

From Table 7, it can be seen that the percentage of coefficients accompanying the selection decreases and the fidelity decreases slightly, and the overall fidelity is above 95%. Therefore it is useful to use the large-valued coefficients from the decomposition of the quantum image as the global features of the quantum image.

## 4.3 | Discussion

### 4.3.1 | Comparative analysis of classical image features and quantum image features

For image classification tasks, the processing is performed by classical computers with common computing units such as CPU and GPU, and the dimensionality of image data can be greatly reduced as well as the final classification effect can be improved by corresponding feature processing algorithms. Classical image features contain colour information, location information, texture information etc. These features are stored in classical bits and cannot be directly applied in quantum computing circuits. In contrast, quantum image features are directly converted from classical features in quantum circuits by quantum image feature extraction methods or through quantum coding, and its storage form is quantum state, which is fundamentally different from classical image features.

### 4.3.2 | Fidelity change analysis

The quantum image feature extraction method PSQIFE proposed here is a quantum dual feature extraction algorithm based on the INCQI quantum images. Among the nine classical images, the distribution of pixels is relatively uniform, except for ‘‘Saturn.jpg’’, which has a concentrated distribution. The fidelity of ‘‘Saturn.jpg’’ image changed abruptly from 91.59% to 73.63% when the selection ratio of large value coefficients was reduced to 0.39% in the experiment because of its concentrated pixel distribution, while the fidelity of the other 8 images changed less. Overall, the PSQIFE method has good results in extracting the global features of quantum images.

### 4.3.3 | Compared with the classification effect of CNN on Mnist data set

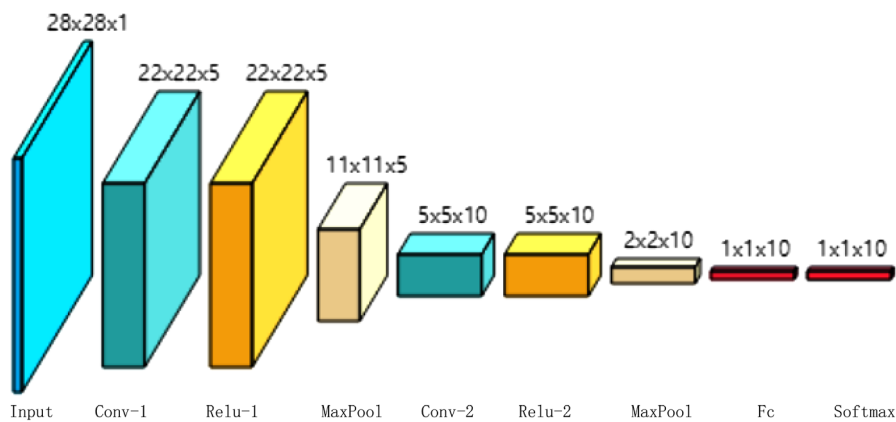
Feature extraction can affect the performance of image classification. The PSQIFE quantum image feature extraction method proposed in this paper and quantum K nearest Neighbour classifier (QKNN) [35] are used to conduct classification experiments on Mnist handwritten digital image data sets [30], and compared with traditional CNN, as shown below (see Table 8). The network structure of the CNN model used is shown in Figure 8.

In Figure 8, Conv-1 and Conv-2 are the convolution layers, Fc is the fully connected layer, and MaxPool is the pooling layer. The superposition of convolutional and pooling layers constitutes the whole feature extraction layer. The output probabilities are mapped from an input image of  $28 \times 28$  size to ten categories through a series of convolution, pooling, and full-connections.

The classification test of this paper is executed on IBM Quantum Experience (IBMQ) [31]. It can be seen from Table 8 that the PSQIFE quantum image feature extraction method has a significant promoting effect on classification.

**TABLE 7** Comparison of fidelity of quantum image reconstruction for different test images

| Coefficient ratio | Fidelity (%) |       |       |       |       |       |       |       |       |       |
|-------------------|--------------|-------|-------|-------|-------|-------|-------|-------|-------|-------|
|                   | (a)          | (b)   | (c)   | (d)   | (e)   | (f)   | (g)   | (h)   | (i)   | (j)   |
| 50%               | 99.17        | 99.90 | 99.96 | 99.95 | 99.89 | 99.95 | 99.72 | 99.98 | 99.91 | 99.83 |
| 25%               | 98.42        | 99.69 | 99.82 | 99.84 | 99.73 | 99.79 | 99.47 | 99.90 | 99.52 | 99.58 |
| 12.5%             | 97.88        | 99.31 | 99.41 | 99.64 | 99.44 | 99.46 | 99.19 | 99.67 | 98.45 | 99.16 |
| 6.25%             | 97.44        | 98.77 | 98.47 | 99.30 | 98.90 | 98.98 | 98.89 | 99.09 | 96.06 | 98.43 |
| 3.125%            | 97.03        | 98.08 | 96.96 | 98.76 | 97.94 | 98.22 | 98.61 | 98.21 | 92.37 | 97.35 |
| 1.56%             | 96.50        | 97.33 | 95.58 | 97.98 | 96.43 | 97.47 | 98.38 | 95.06 | 89.81 | 96.06 |
| 0.78%             | 95.71        | 96.57 | 94.37 | 96.78 | 95.07 | 96.18 | 98.22 | 91.59 | 88.85 | 94.82 |
| 0.39%             | 94.85        | 95.55 | 93.75 | 95.56 | 93.41 | 94.02 | 98.14 | 73.63 | 88.42 | 91.93 |

**FIGURE 8** Specific network structure of CNN**TABLE 8** Compared with the image classification effect of CNN on Mnist data set

| Feature extraction method | Accuracy (%) |
|---------------------------|--------------|
| CNN [25]                  | 97.9%        |
| Ours (PSQIFE)+QKNN        | 97.6%        |

#### 4.3.4 | Dual quantum image global feature extraction analysis

The proposed PSQIFE dual-quantum image global feature extraction method can fully consider the global features of classical images in Euclidean space and the quantum global features in Hilbert space after coding into the INCQI quantum images, giving full play to the fidelity advantage of dual-quantum image features.

Quantum image processing is a new research area combining quantum mechanics and image processing, and there are many issues that deserve in-depth study. Subsequent research continues on effective methods for quantum image feature acquisition, and since direct use of raw image data for classification and recognition leads to time inefficiency and the presence of classification or recognition inaccuracies, quantum image feature

extraction methods similar to classical image feature extraction methods from local and global features of images are carried out. In addition, quantum machine learning methods for image classification and recognition processing are investigated in future work [36–38]. Combining the properties of quantum computing with machine learning algorithms can greatly improve the efficiency of image processing.

## 5 | CONCLUSIONS

Here, we propose a dual quantum image feature extraction method named PSQIFE, which mainly performs the global energy representation of images by constructing dual quantum image global features, where one part of quantum image features is derived from the quantum state encoding of classical image features obtained after PCA transformation of classical images, and the other part of quantum image features is obtained by transforming classical images into INCQI quantum images after the quantum global features are obtained by the SVD-Schmidt decomposition of the INCQI quantum image. The dual quantum image global features are obtained by the quantum superposition of these two parts of quantum state features. The effectiveness of the PSQIFE dual-quantum image feature extraction method is verified through image fidelity tests

on dual-quantum global features as well as classification comparison experiments, which have certain reference significance for quantum image classification.

## ACKNOWLEDGEMENTS

This work was supported by the National Key Research and Development Project of China (grant number: 2016YFD0300710).

## CONFLICT OF INTEREST

The authors declare that they have no known competing financial interests or personal relationships that could have appeared to influence the work reported in this paper.

## DATA AVAILABILITY STATEMENT

The data are available from the corresponding author on reasonable request.

## ORCID

Jie Su  <https://orcid.org/0000-0003-0275-0334>

## REFERENCES

- McAfee, A., Brynjolfsson, E.: Strategy & competition big data: The management revolution. *Harv. Bus. Rev.* 90(10), 60 (2012)
- Li, Y.S., Ma, J.Y., Zhang, Y.J.: Image retrieval from remote sensing big data: A survey. *Inf. Fusion* 67, 94–115 (2021)
- Pouyanfar, S., Yang, Y.M., Chen, S.C., Shyu, M.L., Iyengar, S.S.: Multimedia big data analytics: A survey. *ACM Comput. Surv.* 51(1), 1–34 (2018)
- Deng, J., Dong, W., Socher, R., Li, L.J., Li, K., Li, F.F.: ImageNet: A large-scale hierarchical image database. In: *Cipr: 2009 Ieee Conference on Computer Vision and Pattern Recognition* 1–4, Miami, FL, USA pp. 248–255 (2009)
- Xi, Z., Kai, Y., Tong, Z., Huang, T.S.: Image classification using super-vector coding of local image descriptors. In: *Computer Vision-ecv- european Conference on Computer Vision*, pp. 141–154 (2010)
- Lu, D., Weng, Q.: A survey of image classification methods and techniques for improving classification performance. *Int. J. Remote Sens.* 28(5), 823–870 (2007)
- Wang, W., et al.: Pyramid vision transformer: A versatile backbone for dense prediction without convolutions. In: *Proceedings of the IEEE/CVF International Conference on Computer Vision*, pp. 568–578 (2021)
- Vaswani, A., et al.: Attention is all you need. *Adv. Neural Inf. Process. Syst.* 30, 1–11 (2017)
- Liu, Z., et al.: Swin transformer: Hierarchical vision transformer using shifted windows. In: *Proceedings of the IEEE/CVF International Conference on Computer Vision*, pp. 10012–10022 (2021)
- Touvron, H., Cord, M., Douze, M., Massa, F., Sablayrolles, A., Jégou, H.: Training data-efficient image transformers & distillation through attention. In: *International Conference on Machine Learning. PMLR*, pp. 10347–10357 (2021)
- Ma, L., Zhang, Y.: Research on vehicle license plate recognition technology based on deep convolutional neural networks. *Microprocess. Microsyst.* 82(8), 103932 (2021)
- Chen, M., Peng, H., Fu, J., Ling, H.: Autoformer: Searching transformers for visual recognition. In: *Proceedings of the IEEE/CVF International Conference on Computer Vision*, pp. 12270–12280 (2021)
- Yu, F., Liu, Y.: A sparse feature extraction method based on improved quantum evolutionary algorithm (in Chinese). *Trans. Beijing Inst. Technol.* 40(05), 512–518 (2020)
- Wang, H.: Quantum Information Measurement and Application of Image Processing Based on Nuclear Magnetic Resonance System. University of Science and Technology of China, Hefei, Anhui Province, China (2017)
- Tian, Y., Wang, H.: Image edge feature extraction research based on quantum kernel clustering algorithm (in Chinese). *Acta Metrologica Sinica* 37(06), 582–586 (2016)
- Yi, Z.: Research on Quantum Algorithms for Image Processing. National University of Defense Technology, Changsha, Hunan Province, China (2014)
- Jun, C.: The Research of Affective State Recognition from Electrocardiography Signal Based on QPSO Algorithm. Southwest University, Chongqing, China (2012)
- Li, C.: Research on Technology of Fingerprint Identification Based on Quantum Neural Network. Nanjing University of Posts and Telecommunications, Nanjing, Jiangsu Province, China (2011)
- Zhang, Z.: Image Recognition Based on Quantum-Inspired Synergetic Neural Network. Xidian University, Xi'an, Shaanxi Province, China (2010)
- Yan, W.: Research on Technology of Face Recognition Based on QGA-BP Neural Network. Suzhou University, Suzhou, Jiangsu Province, China (2008)
- Zhou, R., Yang, S., Xu, X.: Pattern feature extraction algorithm based on quantum Fourier transform (in Chinese). *J. Nanjing Univ. Aeronaut. Astronaut.* 40(1), 134–136 (2008)
- Rajesh, V., Naik, U.P., Mohana: Quantum convolutional neural networks (QCNN) using deep learning for computer vision applications. In: *2021 International Conference on Recent Trends on Electronics, Information, Communication & Technology (RTEICT)*, pp. 728–734 (2021)
- Liu, J., Lim, K.H., Wood, K.L., Huang, W., Guo, C., Huang, H.-L.: Hybrid quantum-classical convolutional neural networks. *Sci. China. Phys. Mech. Astron.* 64(9), 1–8 (2021)
- Jing, Y., et al.: RGB image classification with quantum convolutional ansatz. *Quantum Inf. Process.* 21(3), 1–19 (2022)
- Dou, T., Zhang, G., Cui, W.: Efficient quantum feature extraction for CNN-based learning. *arXiv:2201.01246* (2022)
- Bartlett, M.S., Movellan, J.R., Sejnowski, T.J.: Face recognition by independent component analysis. *IEEE Trans. Neural Networks* 13(6), 1450–1464 (2002)
- Scholkopf, B., Smola, A.: Kernel principal component analysis. In: *International Conference on Artificial Neural Networks*, pp. 583–588 (1997)
- Yang, J., Zhang, D., Frangi, A.F., Yang, J.Y.: Two-dimensional PCA: A new approach to appearance-based face representation and recognition. *IEEE Trans. Pattern Anal. Mach. Intell.* 26(1), 131–137 (2004)
- Su, J., Guo, X., Liu, C., Lu, S., Li, L.: An improved novel quantum image representation and its experimental test on IBM quantum experience. *Sci. Rep.* 11(1), 1–13 (2021)
- Kerenidis, I., Luongo, A.: Classification of the MNIST data set with quantum slow feature analysis. *Phys. Rev. A* 101(6), 062327 (2020)
- IBMQ. IBM Quantum Experience. <https://quantum-computing.ibm.com/> (2022). Accessed 15 April 2022
- Sidiropoulos, N.D., De Lathauwer, L., Fu, X., Huang, K., Papalexakis, E.E., Faloutsos, C.: Tensor decomposition for signal processing and machine learning. *IEEE Trans. Signal Process.* 65(13), 3551–3582 (2017)
- Hong, D., Kolda, T.G., Duersch, J.A.: Generalized canonical polyadic tensor decomposition. *SIAM Rev.* 62(1), 133–163 (2020)
- Montangero, S., Montangero, Evenson: Introduction to Tensor Network Methods. Springer, Berlin (2018)
- Basheer, A., Afham, A., Goyal, S.K.: Quantum k-nearest neighbors algorithm. *arXiv:09187* (2020)
- Blank, C., Park, D.K., Rhee, J.-K.K., Petruccione, F.: Quantum classifier with tailored quantum kernel. *npj Quantum Inf.* 6(1), 1–7 (2020)
- Grant, E., et al.: Hierarchical quantum classifiers. *npj Quantum Inf.* 4(1), 1–8 (2018)
- Felser, T., et al.: Quantum-inspired machine learning on high-energy physics data. *npj Quantum Inf.* 7(1), 1–8 (2021)

**How to cite this article:** Su, J., Lu, S., Li, L.: A dual quantum image feature extraction method: PSQIFE. *IET Image Process.* 16, 3529–3543 (2022). <https://doi.org/10.1049/ipr2.12561>